Supplementary Materials to "A Hybrid ℓ_1-ℓ_0 Layer Decomposition Model for Tone mapping"

Zhetong Liang[1], Jun Xu[1], David Zhang[1], Zisheng Cao[2], Lei Zhang[1,*]
[1]The Hong Kong Polytechnic University, [2]DJI Co.,Ltd
zhetong.liang@connect.polyu.hk, csjunxu@comp.polyu.edu.hk, csdzhang@comp.polyu.edu.hk
zisheng.cao@dji.com, cslzhang@comp.polyu.edu.hk

In this supplementary file, we provide:
1. The optimization procedures for solving the hybrid ℓ_1-ℓ_0 decomposition model.
2. More descriptions about the subjective experiments.
3. More visual comparisons of tone mapping results on our HDR database.

1. Solving the Hybrid ℓ_1-ℓ_0 Decomposition Model

As demonstrated in the main paper, the matrix-vector form of the hybrid ℓ_1-ℓ_0 decomposition model is

$$\min_{\boldsymbol{b}} \frac{1}{2}\|\boldsymbol{s}-\boldsymbol{b}\|_2^2 + \lambda_1\|\nabla \boldsymbol{b}\|_1 + \lambda_2 \mathbf{1}^\top F(\nabla(\boldsymbol{s}-\boldsymbol{b})), \tag{1}$$

where $\boldsymbol{s}, \boldsymbol{b} \in \mathbb{R}^N$ are vector variables denoting the original image and the base layer, respectively. ∇ denotes the concatenation of two gradient operator matrices $\nabla = [\nabla_x^\top, \nabla_y^\top]^\top \in \mathbb{R}^{2N\times N}$. $\mathbf{1} \in \mathbb{R}^{2N}$ is a vector of all ones. $F(.)$ is an element-wise indicating function, which outputs ones when the entries of $\nabla(\boldsymbol{s}-\boldsymbol{b})$ are non-zeros, and outputs zeros otherwise.

The objective function (1) cannot be solved directly due to the complicated ℓ_1 and ℓ_0 gradient sparsity terms. We introduce two auxiliary variables, $\boldsymbol{c}_1$, $\boldsymbol{c}_2 \in \mathbb{R}^{2N}$, so that the hybrid ℓ_1-ℓ_0 decomposition model can be reformulated as a linear equality-constrained problem with three variables $\boldsymbol{b}$, $\boldsymbol{c}_1$, $\boldsymbol{c}_2$:

$$\begin{aligned} &\min_{\boldsymbol{b},\boldsymbol{c}_1,\boldsymbol{c}_2} \frac{1}{2}\|\boldsymbol{s}-\boldsymbol{b}\|_2^2 + \lambda_1\|\boldsymbol{c_1}\|_1 + \lambda_2 \mathbf{1}^\top F(\boldsymbol{c_2}), \\ &\text{s.t.} \qquad \boldsymbol{c_1} = \nabla \boldsymbol{b}, \quad \boldsymbol{c_2} = \nabla(\boldsymbol{s}-\boldsymbol{b}) \end{aligned} \tag{2}$$

We adopt the Alternating Direction Method of Multipliers (ADMM) algorithm [1] to solve the constrained optimization problem. The Augmented Lagrangian function of problem (2) is

$$\begin{aligned} \mathcal{L}(\boldsymbol{b},\boldsymbol{c}_1,\boldsymbol{c}_2,\boldsymbol{y}_1,\boldsymbol{y}_2) = &\tfrac{1}{2}\|\boldsymbol{s}-\boldsymbol{b})\|_2^2 + \lambda_1\|\boldsymbol{c}_1\|_1 + \lambda_2\mathbf{1}^\top F(\boldsymbol{c}_2) + (\boldsymbol{c}_1-\nabla\boldsymbol{b})^\top\boldsymbol{y}_1 \\ &+ \big(\boldsymbol{c}_2-\nabla(\boldsymbol{s}-\boldsymbol{b})\big)^\top\boldsymbol{y_2} + \tfrac{\rho}{2}\big(\|\boldsymbol{c}_1-\nabla\boldsymbol{b}\|_2^2 + \|\boldsymbol{c}_2-\nabla(\boldsymbol{s}-\boldsymbol{b})\|_2^2\big), \end{aligned} \tag{3}$$

where $\boldsymbol{y}_i \in \mathbb{R}^{2N}, i=1,2$ are the Lagrangian dual variables. At iteration k ($k=0,1,...,K$), the function (3) is optimized by minimizing the primal sub-problems with respect to $\boldsymbol{b}$, $\boldsymbol{c}_1$, $\boldsymbol{c}_2$, and maximizing the dual problem with respect to $\boldsymbol{y}_1$, $\boldsymbol{y}_2$ alternatively.

(1) Solving $\boldsymbol{b}^{k+1}$ while fixing the others.

Firstly we split vector $\boldsymbol{c}_1^k$ into two equal-length pieces, i.e., $\boldsymbol{c}_1^k = [\boldsymbol{c}_{1,1}^{k\top}, \boldsymbol{c}_{1,2}^{k\top}]^\top$, where $\boldsymbol{c}_{1,i}^k \in \mathbb{R}^N, i=1,2$. In the same fashion, $\boldsymbol{c}_2^k$ is split into $\boldsymbol{c}_{2,1}^k$ and $\boldsymbol{c}_{2,2}^k$, $\boldsymbol{y}_1^k$ into $\boldsymbol{y}_{1,1}^k$ and $\boldsymbol{y}_{1,2}^k$, and $\boldsymbol{y}_2^k$ into $\boldsymbol{y}_{2,1}^k$ and $\boldsymbol{y}_{2,2}^k$. Then the objective function with respect to $\boldsymbol{b}^{k+1}$ is a quadratic programming problem

$$\begin{aligned} \boldsymbol{b}^{k+1} = \arg\min_{\boldsymbol{b}} \Bigg\{ &\frac{1}{2}\|\boldsymbol{s}-\boldsymbol{b}\|_2^2 + \frac{\rho^k}{2}\|\boldsymbol{c}_{1,1}^k - \nabla_x\boldsymbol{b} + \frac{\boldsymbol{y}_{1,1}^k}{\rho^k}\|_2^2 + \frac{\rho^k}{2}\|\boldsymbol{c}_{1,2}^k - \nabla_y\boldsymbol{b} + \frac{\boldsymbol{y}_{1,2}^k}{\rho^k}\|_2^2 \\ &+ \frac{\rho^k}{2}\|\boldsymbol{c}_{2,1}^k - \nabla_x(\boldsymbol{s}-\boldsymbol{b}) + \frac{\boldsymbol{y}_{2,1}^k}{\rho^k}\|_2^2 + \frac{\rho^k}{2}\|\boldsymbol{c}_{2,2}^k - \nabla_y(\boldsymbol{s}-\boldsymbol{b}) + \frac{\boldsymbol{y}_{2,2}^k}{\rho^k}\|_2^2 \Bigg\}, \end{aligned} \tag{4}$$

*This work is supported by HK RGC GRF grant (PolyU 152124/15E) and China NSFC grant (no. 61672446) and DJI donation.

which can be efficiently solved in Fourier domain

$$\boldsymbol{b}^{k+1}=\text{fft}^{-1}\left(\frac{\text{fft}(\boldsymbol{s})+\text{fft}^*(\nabla_x)\cdot\boldsymbol{fx}^k+\text{fft}^*(\nabla_y)\cdot\boldsymbol{fy}^k}{1+2\rho^k(\text{fft}^*(\nabla_x)\cdot\text{fft}(\nabla_x)+\text{fft}^*(\nabla_y)\cdot\text{fft}(\nabla_y))}\right), \tag{5}$$

where

$$\begin{aligned}\boldsymbol{fx}^k &=\text{fft}\left(\rho^k(\boldsymbol{c}_{1,1}^k+\frac{\boldsymbol{y}_{1,1}^k}{\rho^k}+\nabla_x\boldsymbol{s}-\boldsymbol{c}_{2,1}^k-\frac{\boldsymbol{y}_{2,1}^k}{\rho^k})\right),\\ \boldsymbol{fy}^k &=\text{fft}\left(\rho^k(\boldsymbol{c}_{1,2}^k+\frac{\boldsymbol{y}_{1,2}^k}{\rho^k}+\nabla_y\boldsymbol{s}-\boldsymbol{c}_{2,2}^k-\frac{\boldsymbol{y}_{2,2}^k}{\rho^k})\right).\end{aligned} \tag{6}$$

The denotations fft, fft^*, and fft^{-1} are the 2-D FFT, conjugate FFT and inverse FFT, respectively.

(2) Solving $\boldsymbol{c}_1^{k+1}$. The objective function with respect to $\boldsymbol{c}_1^{k+1}$ is

$$\boldsymbol{c}_1^{k+1}=\arg\min_{\boldsymbol{c}_1}\left\{\frac{2\lambda_1}{\rho^k}\|\boldsymbol{c}_1\|_1+\|\boldsymbol{c}_1-\nabla\boldsymbol{b}^{k+1}+\frac{\boldsymbol{y}_1^k}{\rho^k}\|_2^2\right\}, \tag{7}$$

which can be solved by soft-shrinkage operation:

$$\boldsymbol{c}_1^{k+1}=\mathcal{T}_{\lambda_1/\rho^k}(\nabla\boldsymbol{b}^{k+1}-\boldsymbol{y}_1^k/\rho^k), \tag{8}$$

where $\mathcal{T}_\alpha(x)=\text{sign}(x)\cdot\max(|x|-\alpha,0)$ is the soft-thresholding function.

(3) Solving $\boldsymbol{c}_2^{k+1}$.

The objective function with respect to $\boldsymbol{c}_2^{k+1}$ is:

$$\boldsymbol{c}_2^{k+1}=\arg\min_{\boldsymbol{c}_2}\left\{\frac{2\lambda_2}{\rho^k}F(\boldsymbol{c}_2)+(\boldsymbol{c}_2-\boldsymbol{q}^k)^2\right\},\quad\text{where}\quad \boldsymbol{q}^k=\nabla(\boldsymbol{s}-\boldsymbol{b}^{k+1})-\frac{\boldsymbol{y}_2^k}{\rho^k}. \tag{9}$$

This objective function can be solved in an element-wise manner

$$\sum_{j=1}^{2N}\min_{\boldsymbol{c}_{2,j}}\left\{\frac{2\lambda_2}{\rho^k}F(\boldsymbol{c}_{2,j})+(\boldsymbol{c}_{2,j}-\boldsymbol{q}_j^k)^2\right\}, \tag{10}$$

where j is the entry index of a vector. The solution of each scalar function in (10) is

$$\boldsymbol{c}_{2,j}=\begin{cases}0, & \text{if } (\boldsymbol{q}_j^k)^2\le\frac{2\lambda_2}{\rho^k}\\ \boldsymbol{q}_j^k, & \text{Otherwise}\end{cases}. \tag{11}$$

This can be proved as follows:

Proof. Denote by E_j the value of the jth scalar function in (10)

$$E_j=\frac{2\lambda_2}{\rho^k}F(\boldsymbol{c}_{2,j})+(\boldsymbol{c}_{2,j}-\boldsymbol{q}_j^k)^2. \tag{12}$$

1) When $\frac{2\lambda_2}{\rho^k}\ge(\boldsymbol{q}_j^k)^2$, the function value for non-zero $\boldsymbol{c}_{2,j}$ is

$$E_j(\boldsymbol{c}_{2,j}\ne 0)=\frac{2\lambda_2}{\rho^k}+(\boldsymbol{c}_{2,j}-\boldsymbol{q}_j^k)^2\ge\frac{2\lambda_2}{\rho^k}\ge(\boldsymbol{q}_j^k)^2. \tag{13}$$

On the other hand, the function value for the zero-valued $\boldsymbol{c}_{2,j}$ is

$$E_j(\boldsymbol{c}_{2,j}=0)=(\boldsymbol{q}_j^k)^2. \tag{14}$$

Since $E_j(\boldsymbol{c}_{2,j}\ne 0)\ge(\boldsymbol{q}_j^k)^2\ge E_j(\boldsymbol{c}_{2,j}=0)$, the solution is $\boldsymbol{c}_{2,j}=0$ when $\frac{2\lambda_2}{\rho^k}\ge(q_j^k)^2$.

2) When $\frac{2\lambda_2}{\rho^k}<(\boldsymbol{q}_j^k)^2$, Eq. (14) still holds. On the other hand, for non-zero $\boldsymbol{c}_{2,j}$, $E_j(\boldsymbol{c}_{2,j}\ne 0)$ has a minimum of $\frac{2\lambda_2}{\rho^k}$ at $\boldsymbol{c}_{2,j}=\boldsymbol{q}_j^k$. Because $E_j(\boldsymbol{c}_{2,j}=\boldsymbol{q}_j^k)=\frac{2\lambda_2}{\rho^k}\le(\boldsymbol{q}_j^k)^2=E_j(\boldsymbol{c}_{2,j}=0)$, the solution is $\boldsymbol{c}_{2,j}=\boldsymbol{q}_j^k$ when $\frac{2\lambda_2}{\rho^k}<(\boldsymbol{q}_j^k)^2$. $\square$

(4) Dual ascend updates:

$$\begin{aligned}\boldsymbol{y}_1^{k+1}&=\boldsymbol{y}_1^k+\rho^k(\boldsymbol{c}_1^{k+1}-\nabla\boldsymbol{b}^{k+1}),\\ \boldsymbol{y}_2^{k+1}&=\boldsymbol{y}_2^k+\rho^k(\boldsymbol{c}_2^{k+1}-\nabla(\boldsymbol{s}-\boldsymbol{b}^{k+1})).\end{aligned} \tag{15}$$

(5) Update ρ^{k+1} as $\rho^{k+1}=2\rho^k$.

2. More descriptions about the Subjective experiments

In the subjective experiment, as described in the main paper, 6 subjects including 3 males and 3 females were requested to rate the tone mapping results of each tone mapper in the score range from 1 (the worst) to 8 (the best) spaced by 0.5. Two of the six subjects are computer vision researchers, while the others major in other fields. The subjective experiments were conducted in an indoor environment with stable lighting. The images are shown on a PA328 display of 32 inch (7680×4320). A Matlab graphical interface is designed to exhibit the 7 tone mapping results together with the original HDR radiance map simultaneously on the screen, as illustrated in Fig. 1. The original radiance map is fixed at the top left corner, while the 7 tone mapping results are deployed in random locations. For each tone mapping result, there is a rectangular input box where the subjects can type in the scores. Before the experiment, the subjects were given sufficient instructions on the operation of the interface program. Each subject completed the whole experiment with 40 groups of comparisons in two sessions with a 5-min break between the sessions.

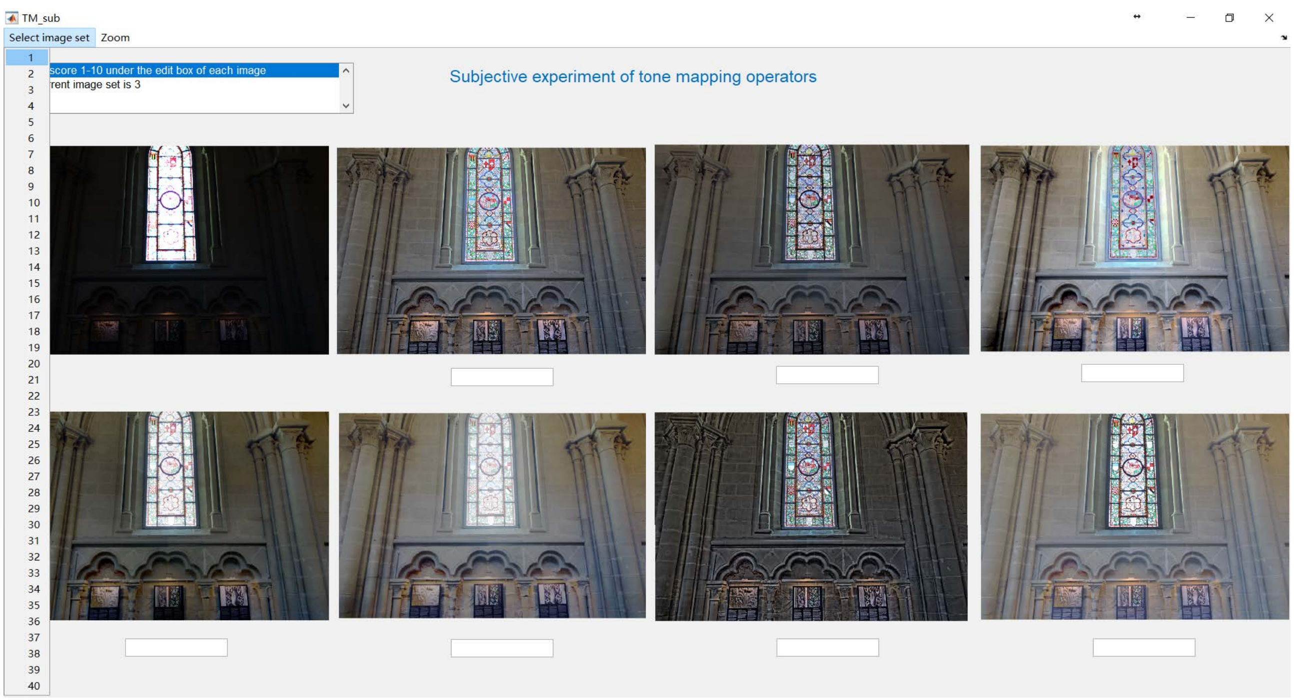

Figure 1. Matlab interface.

3. More Visual Comparisons of Tone Mapping Results

Here we visually compare our tone mapper with the other 6 state-of-the-art tone mappers on 10 radiance maps in our database.

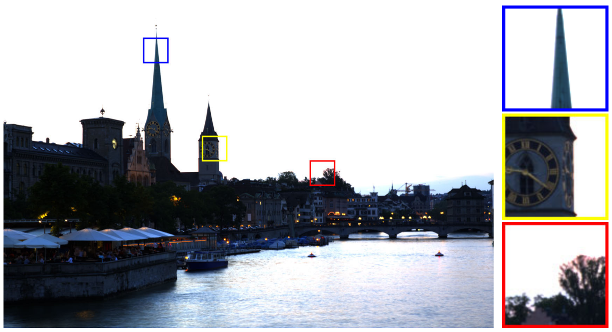

(a) Radiance map

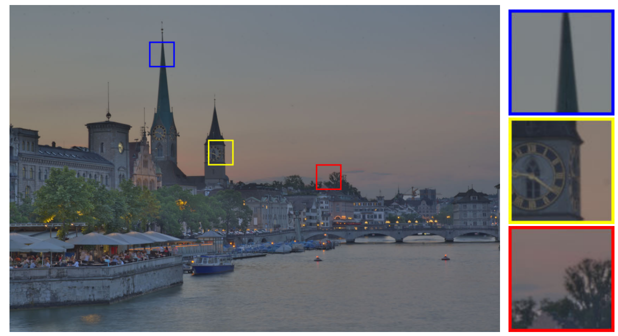

(b) WLS [2]

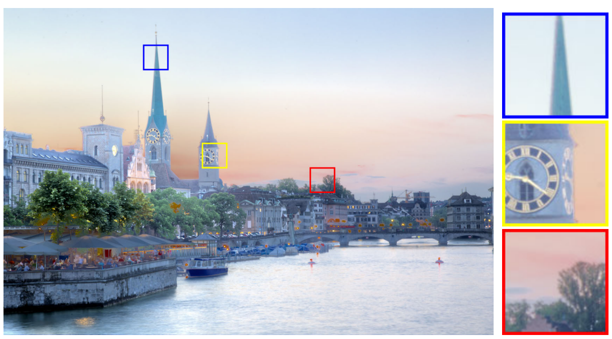

(c) GLW [6]

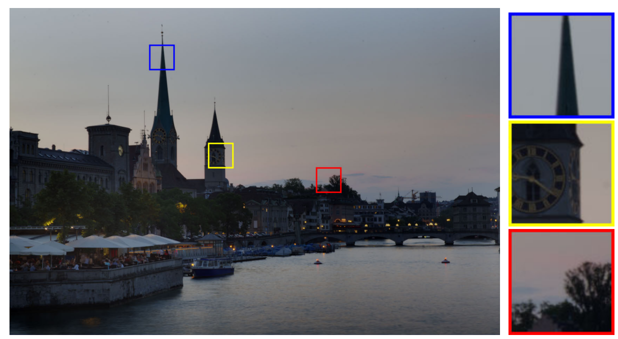

(d) VA [3]

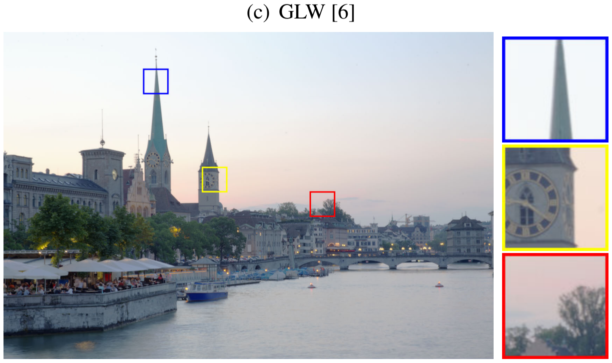

(e) BWC [5]

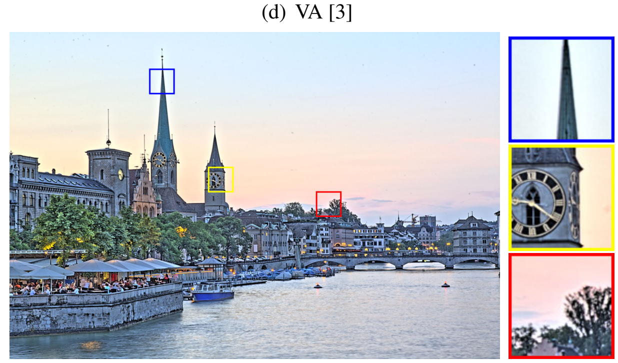

(f) GF [4]

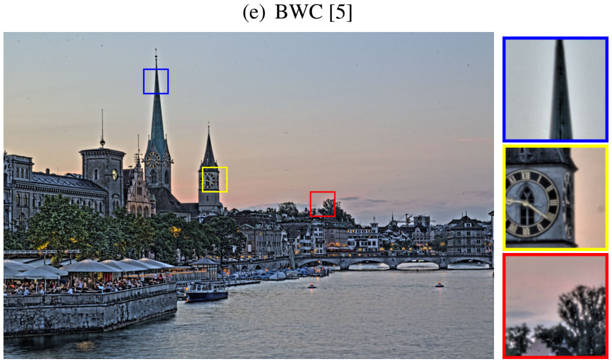

(g) GR [7]

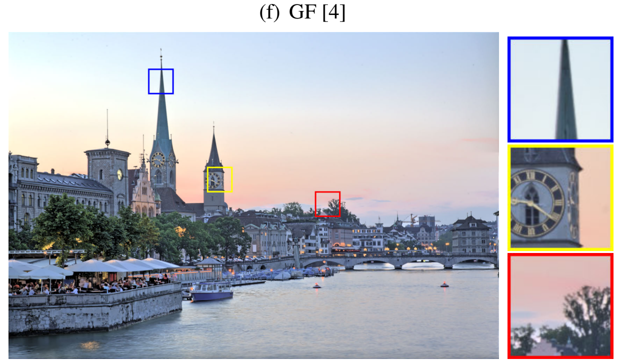

(h) Ours

Figure 2. Comparison of tone mapping results.

(a) Radiance map

(b) WLS [2]

(c) GLW [6]

(d) VA [3]

(e) BWC [5]

(f) GF [4]

(g) GR [7]

(h) Ours

Figure 3. Comparison of tone mapping results.

(a) Radiance map

(b) WLS [2]

(c) GLW [6]

(d) VA [3]

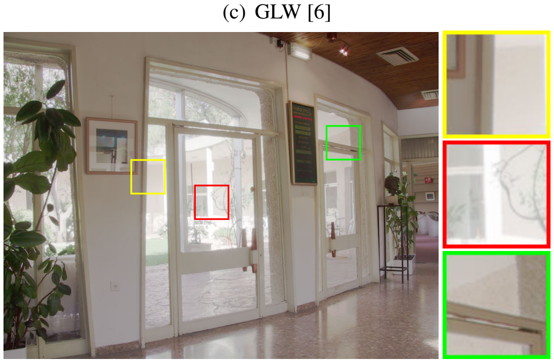

(e) BWC [5]

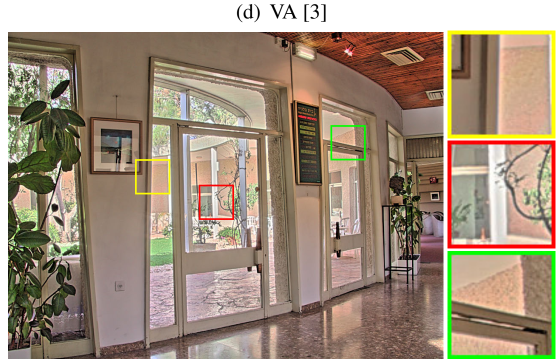

(f) GF [4]

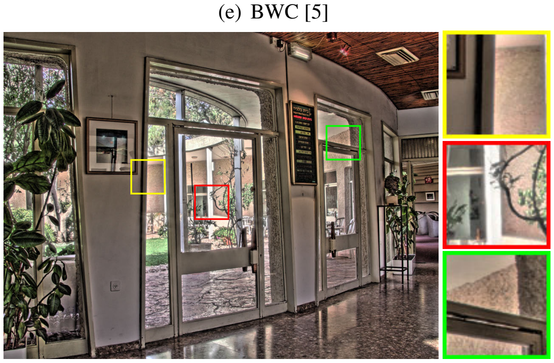

(g) GR [7]

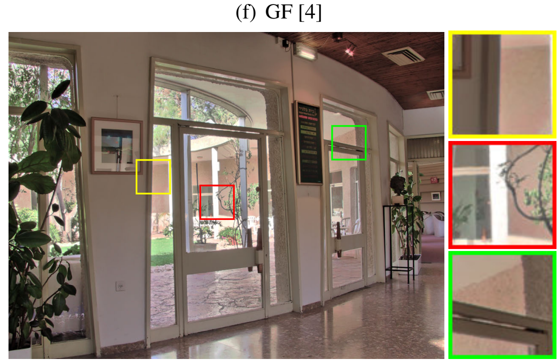

(h) Ours

Figure 4. Comparison of tone mapping results.

(a) Radiance map (b) WLS [2]

(c) GLW [6] (d) VA [3]

(e) BWC [5] (f) GF [4]

(g) GR [7] (h) Ours

Figure 5. Comparison of tone mapping results.

(a) Radiance map

(b) WLS [2]

(c) GLW [6]

(d) VA [3]

(e) BWC [5]

(f) GF [4]

(g) GR [7]

(h) Ours

Figure 6. Comparison of tone mapping results.

(a) Radiance map

(b) WLS [2]

(c) GLW [6]

(d) VA [3]

(e) BWC [5]

(f) GF [4]

(g) GR [7]

(h) Ours

Figure 7. Comparison of tone mapping results.

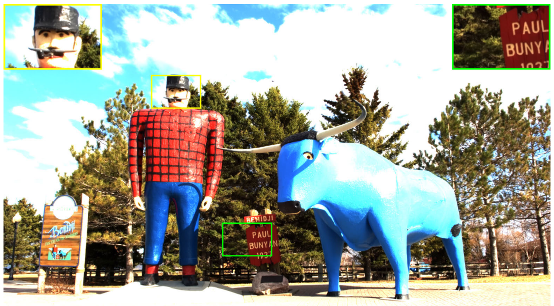

(a) Radiance map

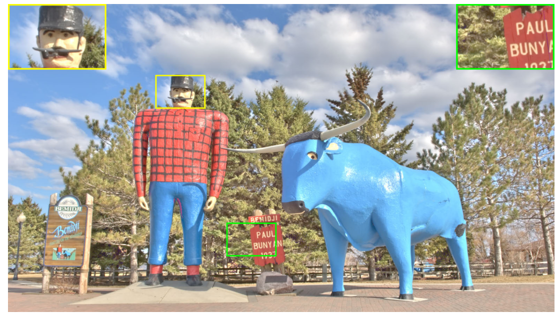

(b) WLS [2]

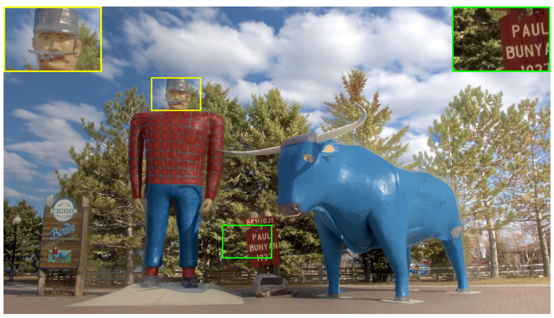

(c) GLW [6]

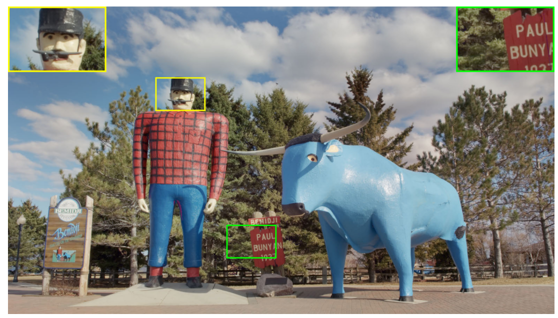

(d) VA [3]

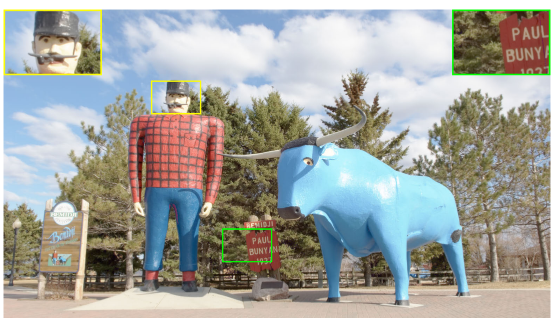

(e) BWC [5]

(f) GF [4]

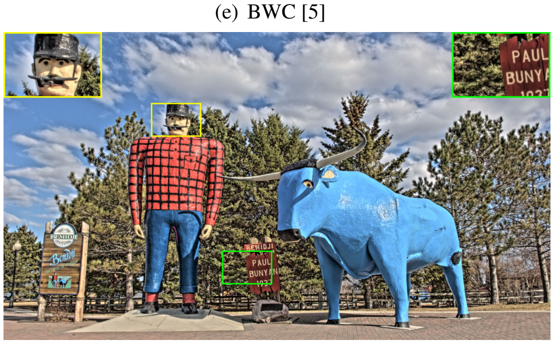

(g) GR [7]

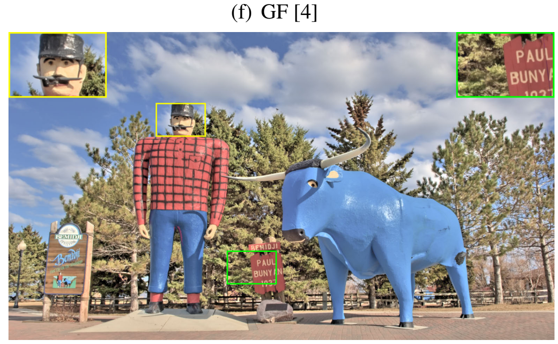

(h) Ours

Figure 8. Comparison of tone mapping results.

(a) Radiance map
(b) WLS [2]
(c) GLW [6]
(d) VA [3]
(e) BWC [5]
(f) GF [4]
(g) GR [7]
(h) Ours

Figure 9. Comparison of tone mapping results.

(a) Radiance map (b) WLS [2]
(c) GLW [6] (d) VA [3]
(e) BWC [5] (f) GF [4]
(g) GR [7] (h) Ours

Figure 10. Comparison of tone mapping results.

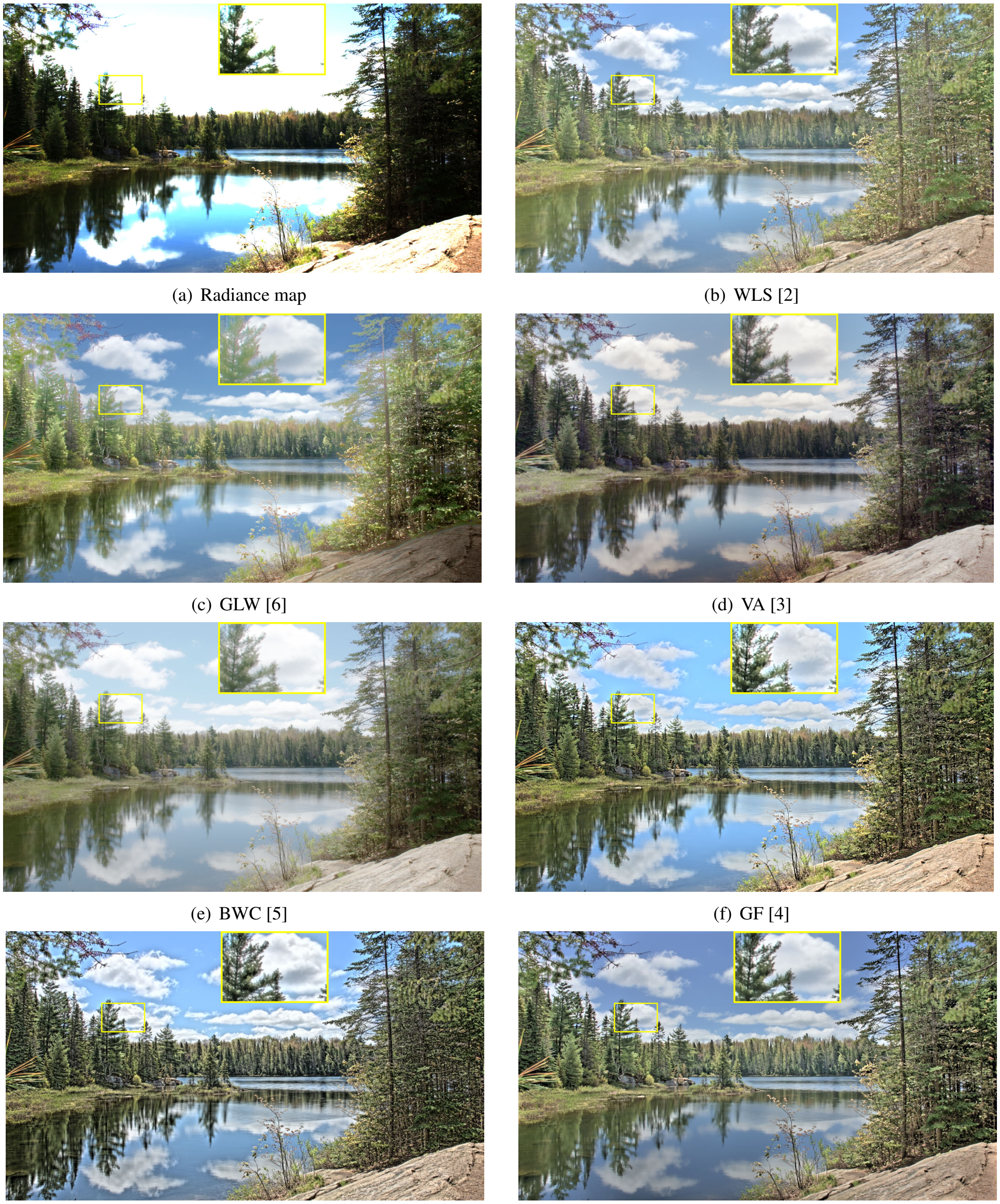

(a) Radiance map

(b) WLS [2]

(c) GLW [6]

(d) VA [3]

(e) BWC [5]

(f) GF [4]

(g) GR [7]

(h) Ours

Figure 11. Comparison of tone mapping results.

References

[1] S. Boyd, N. Parikh, E. Chu, B. Peleato, and J. Eckstein. Distributed optimization and statistical learning via the alternating direction method of multipliers. *Foundations and Trends® in Machine Learning*, 3(1):1–122, 2011.

[2] Z. Farbman, R. Fattal, D. Lischinski, and R. Szeliski. Edge-preserving decompositions for multi-scale tone and detail manipulation. *ACM Trans. Graph.*, 27(3):67:1–67:10, Aug. 2008.

[3] S. Ferradans, M. Bertalmio, E. Provenzi, and V. Caselles. An analysis of visual adaptation and contrast perception for tone mapping. *IEEE Transactions on Pattern Analysis and Machine Intelligence*, 33(10):2002–2012, Oct. 2011.

[4] B. Gu, W. Li, M. Zhu, and M. Wang. Local edge-preserving multiscale decomposition for high dynamic range image tone mapping. *IEEE Transactions on Image Processing*, 22(1):70–79, Jan. 2013.

[5] Z. Mai, H. Mansour, R. Mantiuk, P. Nasiopoulos, R. Ward, and W. Heidrich. Optimizing a tone curve for backward-compatible high dynamic range image and video compression. *IEEE Transactions on Image Processing*, 20(6):1558–1571, June 2011.

[6] Q. Shan, J. Jia, and M. S. Brown. Globally optimized linear windowed tone mapping. *IEEE Transactions on Visualization and Computer Graphics*, 16(4):663–675, July 2010.

[7] T. Shibata, M. Tanaka, and M. Okutomi. Gradient-domain image reconstruction framework with intensity-range and base-structure constraints. In *Proc. IEEE Conf. Computer Vision and Pattern Recognition (CVPR)*, pages 2745–2753, June 2016.